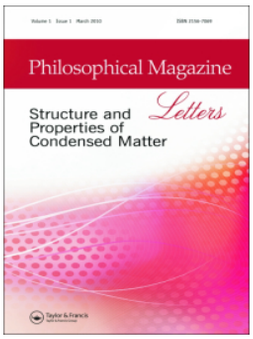

Taylor & Francis
Taylor & Francis Group

Philosophical Magazine Letters

ISSN: (Print) (Online) Journal homepage: https://www.tandfonline.com/loi/tphl20

Notch sensitivity of combined mode I–II fracture behaviour of a rolled magnesium alloy

Dhrubjyoti Baruah, K. V. Vaishakh, S. Arjun Sreedhar, Saurabh Kumar Gupta, Satyam Suwas & R. Narasimhan

To cite this article: Dhrubjyoti Baruah, K. V. Vaishakh, S. Arjun Sreedhar, Saurabh Kumar Gupta, Satyam Suwas & R. Narasimhan (2023) Notch sensitivity of combined mode I–II fracture behaviour of a rolled magnesium alloy, Philosophical Magazine Letters, 103:1, 2173989, DOI: 10.1080/09500839.2023.2173989

To link to this article: https://doi.org/10.1080/09500839.2023.2173989

Published online: 14 Feb 2023.

PHILOSOPHICAL MAGAZINE LETTERS
2023, VOL. 103, NO. 1, 2173989
https://doi.org/10.1080/09500839.2023.2173989

Notch sensitivity of combined mode I–II fracture behaviour of a rolled magnesium alloy

Dhrubjyoti Baruah[a], K. V. Vaishakh[b], S. Arjun Sreedhar[a], Saurabh Kumar Gupta[c], Satyam Suwas [c] and R. Narasimhan[a]

[a]Department of Mechanical Engineering, Indian Institute of Science, Bangalore, India; [b]School of Engineering, Brown University, Providence, RI, USA; [c]Department of Materials Engineering, Indian Institute of Science, Bangalore, India

ABSTRACT

Fatigue pre-cracked four-point bend specimens of a rolled AZ31 Mg alloy are loaded asymmetrically and their mixed-mode (I and II) fracture behaviour is contrasted with pre-notched samples. In-situ mapping of displacement and strain fields is performed through optical imaging coupled with digital image correlation analysis. The fracture surface morphology and the deformed microstructure are also studied. The fracture toughness J_c for both types of specimens is highest for mode I and drops steeply with increase in mode II component. Furthermore, at the same level of mode-mixity, J_c for the notched samples is between two to three times the value pertaining to pre-cracked specimens. This is primarily attributed to quasi-brittle failure, irrespective of mode-mixity, for the latter, whereas the former display a combination of ductile and brittle fracture surface features. At the crack-initiation stage, more profuse tensile twinning is perceived at the far-edge of the ligament in the notched specimens, which also contributes to the observed toughness enhancement.

ARTICLE HISTORY
Received 6 August 2022
Accepted 24 January 2023

KEYWORDS
Mixed-mode fracture; notch sensitivity; magnesium alloy; tensile twinning; fracture toughness

1. Introduction

Magnesium alloys, possess attractive mechanical properties, which makes them suitable candidates for lightweight structural applications [1]. However, besides their poor room-temperature formability, the fracture toughness can also be low [2–4]. This has been attributed to quasi-brittle failure, caused by cracks triggered by twins [5–9]. In contrast, notched specimens of a rolled AZ31 Mg alloy have been observed to exhibit dimple fracture and much higher fracture toughness J_c [10,11]. In references [5,10,11], plastic dissipation induced by

CONTACT R. Narasimhan narasi@iisc.ac.in Department of Mechanical Engineering, Indian Institute of Science, Bangalore 560012, India

$(10\bar{1}2)$ or tensile twins (TTs) was found to contribute substantially to the toughness.

All the experimental investigations referenced above [2–5,10,11] have focussed only on Mode I behaviour. In contrast, mixed-mode fracture response of Mg alloys has received little attention. This assumes importance since structural components can experience combined tension-shear loading during service. Moreover, for engineering alloys, the fracture toughness can either enhance [12] or diminish [13,14] as loading changes from mode I to II. Sharma et al. [15] noted that the mixed-mode (I/III) fracture toughness enhances with addition of mode III component for pure Mg and Mg-Zn alloys while it reduces for Mg-Al alloy.

Vaishakh et al. [16] conducted combined mode (I/II) fracture experiments with asymmetric four-point bend (4-PB) specimens of a rolled AZ31 Mg alloy having notches of diameter 200 μm. They reported a strong decrease in fracture toughness J_c[1] with increase in mode II component. Dimple fracture was perceived under mode I loading whereas shear fracture occurred under mode II. Combination of mode I and II loading causes simultaneous occurrence of both ductile and quasi-brittle failure. In [17], the above trends have been rationalised from crystal plasticity finite element (CPFE) simulations.

The stress state (in particular, triaxiality) can critically affect the failure behaviour, ductility and toughness of Mg alloys [8,11,18]. Mixed-mode loading causes simultaneous sharpening and stretching of the crack/notch surface [13,16,17], thereby leading to significant variation of stresses around the tip. Thus, the triaxiality changes from tension to compression along with intense shearing [17], while the relative magnitudes depend on notch acuity. In view of the above, it is necessary to investigate combined mode I–II fracture behaviour in Mg alloys using fatigue pre-cracked (FPC) specimens and contrast the results with those reported in [16]. This gives motivation for undertaking the present study to examine the following issues for basal-textured Mg alloys.

- For a particular mode-mixity, how does the fracture toughness J_c pertaining to FPC specimen contrast with the notched sample?
- How does mode-mixity affect the failure mechanism for FPC vis-à-vis notched specimens?
- What is the influence of mode-mixity on strain distribution and the development of TTs near the tip as well as in the uncracked ligament for the two types of specimens?

To address the above issues, symmetric and asymmetric four-point bend fracture tests have been conducted on rolled Mg AZ31 alloy using FPC specimens and their fracture behaviour contrasted with that displayed by notched specimens [16]. This is further corroborated with observations from DIC analysis, fractographic study and microstructural characterisation.

2. Experimental procedure

Figure 1a–c illustrates the specimen dimensions and the loading configurations employed in this study. The four-point bend specimens are cut from a 12.7 mm thick rolled AZ31 Mg alloy plate so that the width, $W =$ 10 mm, is along the TD (transverse direction) and the span is along the RD (rolling direction). The chemical composition of the alloy, in weight percent, is 95.89 Mg, 2.75 Al, 1.12 Zn, and 0.14 Mn. A bimodal grain-size distribution is observed from the initial microstructure (see inverse pole figure (IPF) map, Figure 1d) and the average grain size is estimated as 10.8 ± 6 μm. From the (0001) pole figure (Figure 1e) it can be seen that the alloy has a near-basal texture, such that the *c*-axis in most grains is oriented close to the ND (normal direction). In all the specimens, notches of diameter 200 ± 20 μm are introduced up to a depth of 5 mm as in reference [16]. Furthermore, the thickness in the notched section is reduced to 5 mm in order to limit the peak load levels (see Figure 1a–c). Fatigue precracking of the notched samples is carried out to grow cracks from the notch roots up to a length of 0.5 mm. Static experiments are conducted with loading and support rollers placed as shown in Figure 1. S4PBS (Figure 1a) and AS4PB-0S (Figure 1c) pertain to pure modes I and II loading. AS4PB-1S and AS4PB-2S are mixed-mode fracture geometries (a typical specimen of this type is shown in Figure 1b).

The specimens are characterised by the level of elastic mode-mixity parameter M_e. In the AS4PB specimens, the mode-mixity level is varied by changing the distance *d* between the center-line of the specimen and the notch/crack

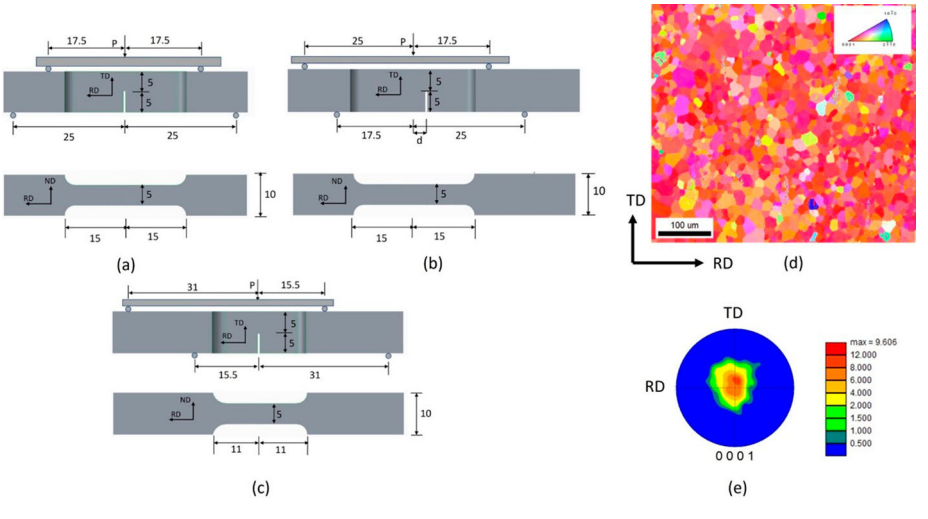

Figure 1. Front and top views showing specimen geometries and dimensions (in mm) for specimens subjected to (a) mode I, (b) mixed-mode and (c) mode II loading. (d) IPF map of undeformed alloy and (e) initial (0001) pole figure.

line (Figure 1b). The values of M_e which is defined by:

$$M_e = \frac{2}{\pi}\tan^{-1}\left(\frac{K_I}{K_{II}}\right), \tag{1}$$

pertaining to all the tested specimens are given in Table 1. In the above expression, K_I and K_{II} denote the stress intensity factors corresponding to opening and in-plane shearing modes, respectively. Thus, $M_e = 1$ for S4PBS (mode I) and varies in the range $0 \leq M_e < 1$ for AS4PBS with $M_e = 0$ representing mode II loading (see Table 1).

Following [19], a near-tip plastic mode-mixity parameter M_p is also defined as:

$$M_p = \frac{2}{\pi}\tan^{-1}\left(\frac{\delta_I}{\delta_{II}}\right)_{r\to 0} \tag{2}$$

Here, δ_I and δ_{II} are notch/crack tip opening and sliding displacements, which in the present work are estimated at a distance of 100 μm behind the tip. The M_p values (averaged over multiple specimens) are found to be 0.49 and 0.33 for AS4PB-2S and AS4PB-1S, which are markedly lower than the corresponding M_e values indicating higher shearing displacement near the tip owing to plastic deformation (Table 1).

All the fracture tests under four-point bending at room temperature are carried out on a servo-hydraulic universal testing machine (UTM) under displacement-controlled mode and the load-point displacement rate is kept constant at 0.001 mm/s. A minimum of three specimens were tested for each case to ensure repeatability. A speckle pattern is sprayed on the specimen surface mainly comprising of black and white dots. A Nikon D7000 DSLR camera is used to obtain optical images of the specimen surface at a resolution of 16 megapixels at every 10 s interval throughout the fracture experiments. The evolution of deformation and strains on the specimen surface are ascertained through Digital Image Correlation (DIC) software (Vic-2D). For DIC analysis, the subset size and step size used (in pixels) are 110×110 and 7 respectively, whereas the strain filter size is chosen as 15. The notch/crack mouth opening and sliding displacements (δ_o and δ_s), as well as the displacements near the tip, δ_I and δ_{II}, are determined from the above DIC analysis. The specimen rotation or notch mouth opening angle (θ) is then computed using the

Table 1. Specimen type, elastic/plastic mode mixity M_e/M_p and J_c values.

Specimen type	M_e	M_p	J_c Notched (N/mm)	J_c FPC (N/mm)
S4PBS	1	1	65 ± 2	32 ± 2
AS4PB-2S	0.85	0.49	52 ± 1	25 ± 1
AS4PB-1S	0.71	0.33	46 ± 1	16 ± 1
AS4PB-0S	0	0	30 ± 1	12 ± 1

expression:

$$\theta = \frac{\delta_o}{a + rb} \tag{3}$$

where, a and b represent the lengths of the total notch/crack and the uncracked ligament respectively. Further, r represents a factor which locates the plastic hinge point on the ligament and lies in the range $0 < r < 1$. This factor is obtained from DIC analysis by examining the normal strain distribution.

The total energy release rate J is taken to be the sum of two components, J_I and J_{II} as:

$$J = J_I + J_{II}. \tag{4}$$

Here, J_I and J_{II} are expressed as:

$$J_I = \frac{\eta_I}{Bb} \int_0^\theta M d\theta, \tag{5}$$

and

$$J_{II} = \frac{\eta_{II}}{Bb} \int_0^{\delta_s} V d\delta_s, \tag{6}$$

where, M and V are bending moment and shear force on the ligament, and B is the specimen thickness. Vaishakh and Narasimhan [19] had validated the above procedure through detailed finite-element analysis, and estimated the values of the factors η_I and η_{II} as 2 and 1, respectively.

The fracture toughness, J_c, is ascertained from the recorded J versus load variation after identifying the crack initiation stage through careful visual observation of the in-situ images. This is verified by observing the normal strain distribution near the pre-crack tip, which attains a peak value at crack initiation stage. Further confirmation of the estimated toughness is obtained by extrapolating the resistance curves (J versus Δa) to $\Delta a = 0$ as suggested in reference [20] for mode-I fracture testing.

In some of the tests, the specimens after crack initiation are subjected to microstructural investigations (optical metallography and EBSD) and fractographic study using a scanning electron microscope (SEM). Specimen surface preparation for optical metallography and EBSD is done following the same methodology employed in reference [21]. Fractography of the completely broken specimens are conducted immediately after the tests to prevent oxidation.

3. Results and discussion

The fracture toughness J_c corresponding to all specimens is summarised in Table 1. A dramatic decrease in J_c (by factors of 2.17 and 2.67 for notched and FPC specimens respectively) from mode I to II loading is observed. At the same M_e, the former exhibits significantly higher J_c compared to the latter (by a factor of 2 for mode I and 2.5 for mode II). In order to understand these trends, detailed analyses of the fracture surface morphology, the strain distribution, and the deformed microstructure are described below.

In Figure 2, SEM images of the fracture surface for the FPC and the notched specimens pertaining to M_e (M_p) of 0.85 (0.49) and 0.71 (0.33) are presented. The FPC samples display elongated grooves or step-like ridges (locations C and D in Figure 2a and H in Figure 2c). Such quasi-brittle features, observed for all FPC specimens, have been reported earlier only under mode I loading [3,11,21]. They have been classified as Cleavage 3 failure [22] and are associated with cracks nucleated at twin-twin intersections or along twin boundaries [3,5]. This implies that the propensity for operation of the above failure mechanism depends on the evolution rate of TTs near the tip.

On the other hand, for notched AS4PB-2S (Figure 2b), ductile fracture features, consisting of large, rounded dimples (e.g. location E) with some enclosing inclusions (e.g. G) along with few tear ridges (e.g. F) are observed. Similar

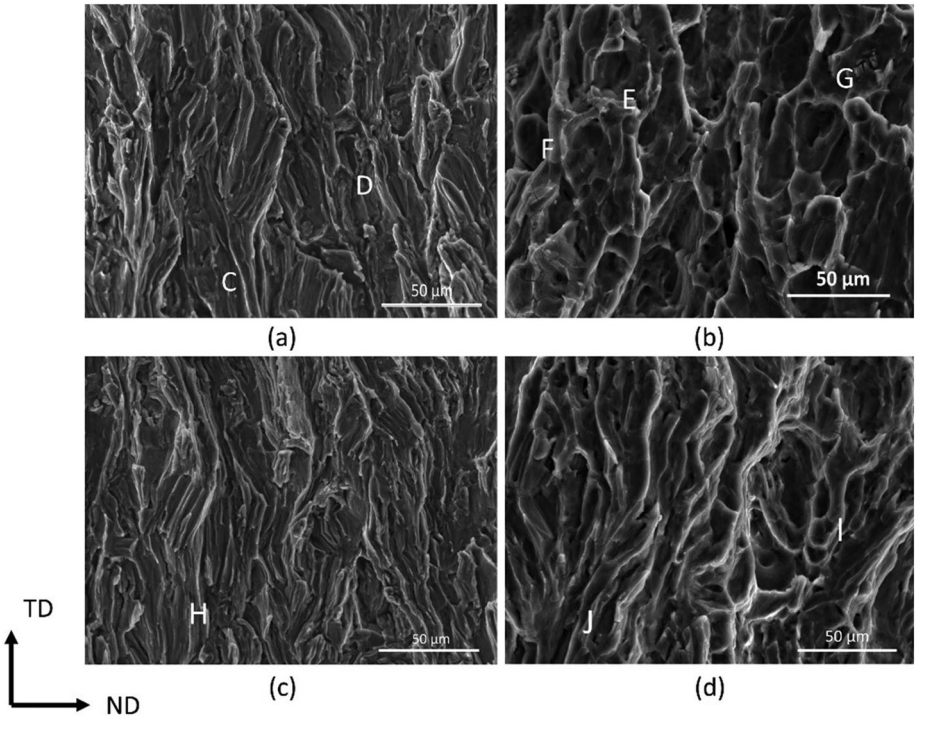

Figure 2. SEM fractographs for AS4PB-2S with (a) FPC and (b) notch. Similar images for AS4PB-1S with (c) FPC and (d) notch. Crack growth direction is vertically upwards.

morphology was seen for notched S4PBS. The notched AS4PB-1S (see Figure 2d) exhibits a hybrid mechanism consisting of elongated dimples (e.g. I) and step-like ridges (e.g. J). However, the fracture surface of the notched AS4PB-0S is found to be heavily sheared with no clear features [16].

Figure 3a and c show optical micrographs following crack initiation stages in FPC and notched AS4PB-2S respectively, taken near the notch/crack tip. Numerous TTs and TT-TT intersections (more for the former) in the grains adjacent to the crack surface can be noticed for both specimens (see Figure 3b and d, which are enlarged views of the regions marked in Figure 3a and c, respectively). In Figure 3b, a few TTs and TT-TT intersections are marked as O and P respectively. On the other hand, Q and R in Figure 3d indicate few TTs and TT-TT intersections respectively. By employing the point count method [23], the average TT area fraction, $\bar{f}_{tt}$, is calculated considering the images shown in Figure 3b and d as 13% and 6%, respectively. On using the corresponding J_c values (Table 1), the average evolution rates of $\bar{f}_{tt}$ with respect to J for the above two specimens are estimated to be 0.0052 and 0.0012 mm/N. Thus, a faster TT accumulation rate near the tip occurs for the FPC sample, which triggers twin-induced quasi-brittle failure (Figure 2a). For the notched sample, this mechanism is suppressed owing to sluggish evolution of TTs near the tip giving rise to dimple fracture.

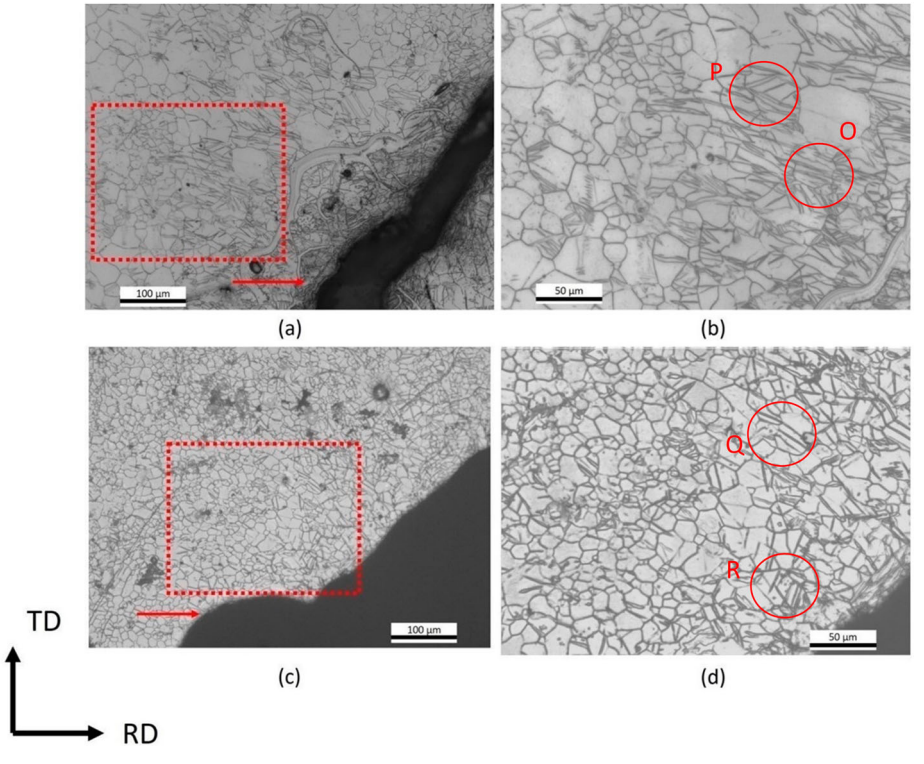

Figure 3. Optical micrographs near the initial tip (indicated by horizontal arrows) for AS4PB-2S with (a) FPC and (c) notch. (b), (d) Enlarged views of the regions marked by boxes in (a) and (c).

Figure 4a and b display Von Mises strain contours for FPC and notched AS4PB-2S, respectively, just prior to crack initiation stages ($J \sim 0.8J_c$). Similar images for the two AS4PB-0S are presented in Figure 4c and d. For AS4PB-2S, two asymmetrical lobes in the strain contours, typical of mixed-mode loading can be seen extending from the tip, thereby indicating a combined tension-shear stress state. Further, perceptible strain accumulation is noticed at the far-edge (see Figure 4a and b). In contrast, the Von Mises strain develops mainly ahead of the tip in AS4PB-0S (Figure 4c and d), with less intensity at the far-edge. Thus, the average Von Mises strain values at the specimen far-edge computed over the boxes marked in Figure 4a and b for the FPC and notched AS4PB-2S are 0.014 and 0.023, whereas they are 0.007 and 0.014 for AS4PB-0S (see boxes in Figure 4c and d). The average values of strain are quantified above to corroborate subsequently with the average TT area fraction at the far-edge of the ligament. On the other hand, the peak levels of Von Mises strain at the specimen far-edge are found to be 0.021 and 0.034 for AS4PB-2 FPC and notched specimens, respectively. For AS4PB-0S, the corresponding values are 0.016 and 0.028, respectively. Thus, the peak strain levels exhibit trends similar to the average values, although as expected they are higher. On the contrary, intense shearing causes higher

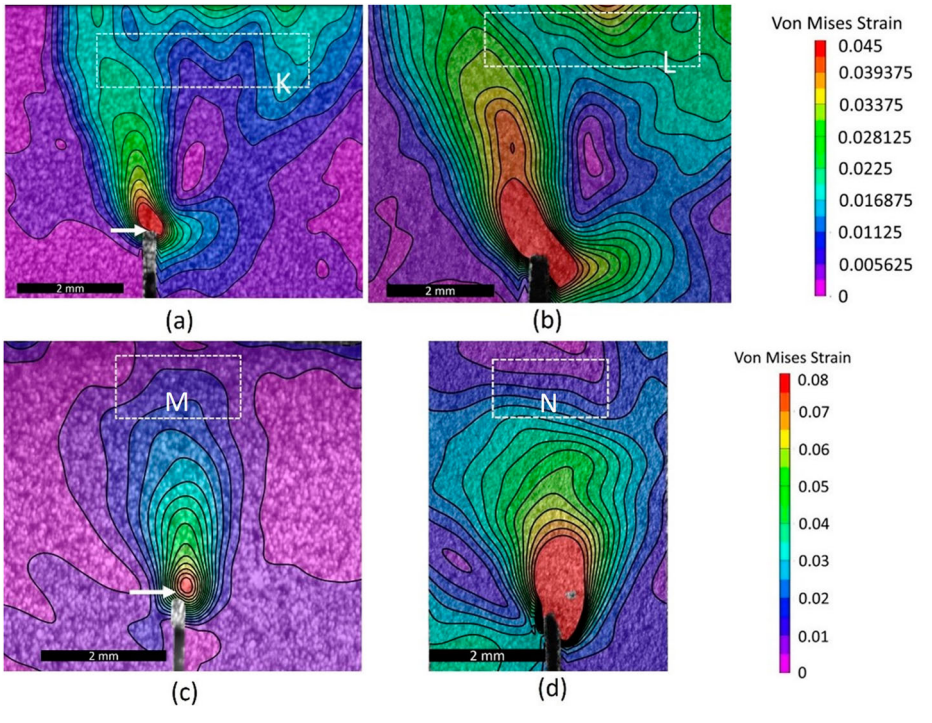

Figure 4. Von Mises strain contours at $J \sim 0.8J_c$ for AS4PB-2S with (a) FPC and (b) notch. Similar contours for AS4PB-0S with (c) FPC and (d) notch. The FPC tip is indicated by white arrows in (a), (c). Average strain values in the rectangular boxes marked in these figures are quantified.

strain concentration near the tip for AS4PB-0S than AS4PB-2S. Further, comparing Figure 4a with b and c with d, the observed near-tip strain levels are more for the notched samples owing to higher J values [17,24].

Figure 5a and b show EBSD IPF and (0001) pole-figure maps at the crack initiation stage for FPC and notched AS4PB-2S taken at locations K and L indicated in Figure 4a and b, respectively. While multiple, parallel TTs are observed from the IPF in several grains in the FPC specimen (Figure 5a), they are wider and more profuse in the notched sample (Figure 5b). This corroborates with more deviation of the (0001) pole figure from the initial one (Figure 1e) for the latter (Figure 5b) as compared to the former (Figure 5a). Also, the above strong difference in TT accumulation near the specimen far-edge between the two types of samples correlates with the overall strain levels in this region (Figure 4a and b). The average TT area fraction, $\overline{f}_{tt}$, for both these cases is estimated from the entire IPF map having dimensions 525 μm × 420 μm. To this end, the twinned regions (identified as having lattice orientation almost perpendicular to the (0001) axis) are first enclosed within polygons using Image-J software and $\overline{f}_{tt}$ is then calculated as $\overline{f}_{tt} = A_{tt}/A$, where A_{tt} is the total area enclosed by TTs and A is the area of the entire IPF map. The values of $\overline{f}_{tt}$, estimated from Figure 5a and b using Image-J software are 19% and 26%, respectively. Figure 5c and d show the IPF and pole figure maps for FPC and notched AS4PB-0S taken at locations M and N indicated in Figure 4c and d, respectively. For this case also, fewer twins can be observed for the FPC sample (Figure 5c) as compared to the notched counterpart (Figure 5d). Thus, the $\overline{f}_{tt}$ values at the far-edge for the FPC and notched samples are found to be 6% and 15% respectively. As in the case of AS4PB-2S, the above results corroborate well both with the texture changes perceived

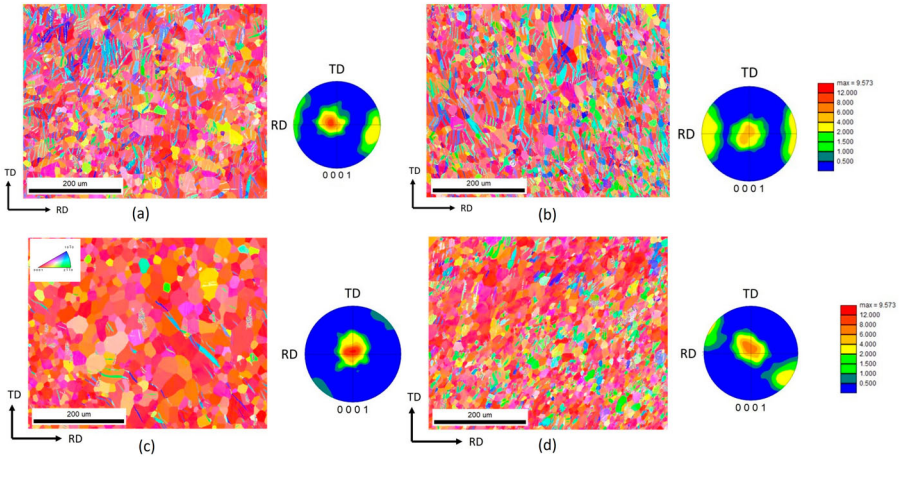

Figure 5. EBSD maps (IPF and pole figures) taken at far-edge of AS4PB-2S (locations K and L in Figure 4a and b) with (a) FPC and (b) notch. (c), (d) Similar maps taken for AS4PB-0S (locations M and N in Figure 4c and d) with FPC and notch.

from the corresponding pole figures (Figure 5c and d) and the overall strain distribution at the specimen far-edge (Figure 4c and d).

In order to rationalise the above results, it should be first noted that J_c, involves contributions from work of separation associated with near-tip fracture processes, J_c^{nt}, and background plastic dissipation, J_c^{bp}. As discussed in reference [25], the competition between quasi-brittle and ductile fracture processes in Mg alloys is governed by the evolution rates of $\bar{f}_{tt}$ and porosity f_v with respect to J near the tip. The former would enhance micro-crack nucleation sites (TT-TT intersections, TT boundaries), which, when subjected to high tensile principal stresses, will potentially trigger early fracture initiation [5,17,25]. Also, higher stress concentration near FPC tips will increase $\bar{f}_{tt}$ evolution rate in comparison to blunt notch tips at the same mode-mixity (for example, by a factor of 4.3 for AS4PB-2S, see Figure 3). Moreover, CPFE simulations [17] showed that a decrease in M_e enhances $\bar{f}_{tt}$ development adjacent to the stretched part of the notch where high tensile principal stresses prevail. Thus, there is greater propensity for quasi-brittle failure near the tip in FPC specimens, at a given M_e (or M_p), and in notched specimens as the mode-mixity parameter is reduced [16,17].

On the other hand, stress triaxiality, plastic strains, twinning and crystallographic orientation can dictate void growth and coalescence in Mg [25–28]. However, a drop in near-tip triaxiality caused by a reduction in M_e is expected to retard it [17]. Interestingly, large, rounded voids are perceived in Figure 2b which pertains to $M_e = 0.85$ ($M_p = 0.49$), whereas few elongated voids are seen in Figure 2d which corresponds to $M_e = 0.71$ ($M_p = 0.33$). This is possibly caused by more TT development for the latter as suggested by CPFE simulations [27]. In any case, the above noted ductile-brittle transitions will have the detrimental effect of diminishing J_c^{nt}.

In the context of Mg alloys, TT-induced dissipation in the background plastic zone contributes substantially to J_c^{bp} (at least 30% [25]). The estimated $\bar{f}_{tt}$ at the ligament far-edge corresponding to crack initiation is lower for FPC than notched specimen by a factor of 1.37 and 2.5 for AS4PB-2S and AS4PB-0S, respectively. This implies that a reduction in J_c^{bp} in FPC specimens with respect to notched ones would be markedly higher under mode-II dominant loading. Furthermore, $\bar{f}_{tt}$ at the far-edge diminishes with M_e. For example, it is lower by factors of 1.73 and 3.17 in notched and FPC AS4PB-0S as compared to corresponding AS4PB-2S specimens. This causes a larger drop in J_c^{bp} for the FPC samples as M_e decreases.

4. Conclusions

In the present work, the fracture behaviour displayed by 4-PB FPC specimens of a rolled AZ31 Mg alloy subjected to mixed-mode (I/II) loading has been contrasted with the behaviour of notched samples. Two important observations

have emerged from the analysis of the results. First, the fracture toughness J_c drops with addition of mode-II component for both these specimens, albeit being more pronounced for the FPC samples. Secondly, irrespective of mode mixity, the FPC samples show markedly lower J_c values compared to their notched counterparts. The DIC, microstructural and fractographic characterisations conducted clearly pinpoint the pivotal role of TTs in influencing these two key results. The average TT evolution in the vicinity of the tip with respect to energy release rate, J, in the FPC samples is much faster than the notched ones. This, in turn, facilitates brittle failure near the tip in FPC samples owing to nucleation of micro-cracks, possibly at twin-twin intersections, which propagate along twin-boundaries giving rise to characteristic elongated groove-like features on the fracture surface. By contrast, slower TT evolution near the tip in the notched samples, especially under mode I dominant loading, suppresses quasi-brittle failure giving rise to dimple fracture. However, a combination of voids and brittle features are perceived on the fracture surface of notched samples when M_e decreases. This may be attributed to strong TT accumulation near the stretched part of the notch as demonstrated by CPFE simulations which enhances the propensity for brittle failure. It is therefore concluded that the occurrence of quasi-brittle failure in the fracture process zone near the tip in FPC samples as opposed to ductile or hybrid failure in the notched specimens is primarily responsible for the reduction in J_c.

In contrast to the above detrimental effect of the TTs forming in the stress concentration zone near the tip, those which develop under the compressive stress field prevailing near the far-edge of the ligament play a benevolent role by promoting dissipation and imparting toughness. Thus, EBSD IPF maps clearly show that more profuse tensile twinning has occurred over the above region in the notched samples than in FPC ones corresponding to crack initiation stage at a fixed level of M_e. This corroborates with texture changes and strain intensity as evidenced from DIC measurements. On the other hand, with decrease in M_e, TT development in the background plastic zone becomes weaker for both notched and FPC samples. Consequently, the above benevolent contribution of TTs to toughening diminishes with reduction in M_e, which is more pronounced for the latter.

The present results are important because mixed-mode loading can occur in many practical situations such as angled cracks in rectangular panels subjected to biaxial loading. Thus, fracture-based design of Mg alloys employing the mode-I fracture toughness can be highly unconservative in such situations. On the other hand, the pronounced enhancement in notched fracture toughness with respect to that pertaining for sharp cracks renders design based on the latter overly conservative, which can be undesirable in light-weight applications such as in aerospace and automobile industries. It is considered that the present results provide useful guidelines for rational design of engineering components employing Mg alloys.

Note

1. Here, the fracture toughness is taken to be the critical value of energy release rate, J_c, corresponding to the stage where a crack has initiated from the deformed notch/pre-crack tip under the application of mixed-mode loading.

Disclosure statement

No potential conflict of interest was reported by the author(s).

Funding

This work was supported by Indian Institute of Science under the Institute of Eminence.

Notes on contributors

Dhrubjyoti Baruah is currently pursuing his Ph.D. in Mechanical Engineering at Indian Institute of Science, Bangalore. He received his B. Tech. degree in Mechanical Engineering from Tezpur University in 2013 and M. Tech. in Automobile Engineering from NIT, Warangal in 2016. His research work involves experimental and numerical studies on mixed-mode fracture behavior of magnesium alloys.

K.V. Vaishakh is a postdoctoral researcher at Brown University. He completed his B. Tech. in Mechanical Engineering from College of Engineering, Trivandrum, M. Tech. in Applied Mechanics from IIT Delhi, and Ph.D. in Mechanical Engineering Department at Indian Institute of Science, Bangalore. His current research interests include fracture behavior of engineering materials and damage mechanics.

S. Arjun Sreedhar is currently pursuing his Ph.D. in Mechanical Engineering at Indian Institute of Science, Bangalore. He received his B. Tech. degree in Mechanical Engineering from Government Engineering College, Thrissur in 2012 and M. Tech. in Machine Design from NIT, Calicut in 2017. His research work involves experimental and numerical studies on high strain rate and temperature effects on mode I fracture behavior of magnesium alloys.

Saurabh Kumar Gupta is a Ph.D. scholar in the Department of Materials Engineering at Indian Institute of Science, Bangalore. He has completed his B. Tech. in Mechanical Engineering from Abdul Kalam Technical University and M. Tech. in Materials Science from IIT, Kanpur. He joined Indian Institute of Science, Bangalore in 2018, as Ph.D. student under the supervision of Prof. Satyam Suwas and Dr. Kaushik Chatterjee. His research work focuses on additive manufacturing of titanium implants for orthopedic applications.

Prof. Satyam Suwas received his Ph.D. from Indian Institute of Technology, Kanpur in 1999. He is currently a professor in Materials Engineering at Indian Institute of Science, Bangalore. His research interests are Processing-texture Relationship, Deformation and Thermo-mechanical Processing, and Microstructure-mechanical Property Correlation.

Prof. R. Narasimhan received his Ph.D. in Applied Mechanics from California Institute of Technology in 1986. He is currently a professor in Mechanical Engineering at Indian Institute of Science, Bangalore. His research interests are Solid Mechanics, Fracture Mechanics, and Mechanical Behavior of Materials.

ORCID

Satyam Suwas http://orcid.org/0000-0002-1722-6650

References

[1] C. Blawert, N. Hort, and K.U. Kainer, *Automotive applications of magnesium and its alloys*. Int. J. Adv. Manuf. Technol. 39 (2004), pp. 851–865.
[2] H. Somekawa, and T. Mukai, *Fracture toughness in a rolled AZ31 magnesium alloy*. J. Alloys Compd. 417 (2006), pp. 209–213.
[3] H. Somekawa, A. Singh, and T. Mukai, *Fracture mechanism of a coarse-grained magnesium alloy during fracture toughness testing*. Philos. Mag. Lett. 89 (2009), pp. 2–10.
[4] H. Somekawa, K. Nakajima, A. Singh, and T. Mukai, *Ductile fracture mechanism in fine-grained alloy*. Philos. Mag. Lett. 90 (2010), pp. 831–839.
[5] V. Kaushik, R. Narasimhan, and R.K. Mishra, *Experimental study of fracture behavior of magnesium single crystals*. Mater. Sci. Eng. A 590 (2014), pp. 174–185.
[6] A.K. Ray, and D.S. Wilkinson, *The effect of microstructure on damage and fracture in AZ31B and ZEK100 magnesium alloys*. Mater. Sci. Eng. A 658 (2016), pp. 33–41.
[7] M.J. Nemcko, and D.S. Wilkinson, *On the damage and fracture of commercially pure magnesium using x-ray microtomography*. Mater. Sci. Eng. A 676 (2016), pp. 146–155.
[8] B. Kondori, and A.A. Benzerga, *Effect of stress triaxiality on the flow and fracture of Mg alloy AZ31*. Metall. Mater. Trans. A Phys. Metall. Mater. Sci. 45 (2014), pp. 3292–3307.
[9] A.K. Rodriguez, G.A. Ayoub, B. Mansoor, and A.A. Benzerga, *Effect of strain rate and temperature on fracture of magnesium alloy AZ31B*. Acta Mater. 112 (2016), pp. 194–208.
[10] N.S. Prasad, N. Naveen Kumar, R. Narasimhan, and S. Suwas, *Fracture behavior of magnesium alloys-Role of tensile twinning*. Acta Mater. 94 (2015), pp. 281–293.
[11] N.S. Prasad, R. Narasimhan, and S. Suwas, *Effect of notch acuity on the fracture behavior of AZ31 Mg alloy*. Eng. Fract. Mech. 187 (2018), pp. 241–261.
[12] N. Hallbäck, and F. Nilsson, *Mixed-mode I/II fracture behavior of an aluminium alloy*. J. Mech. Phys. Solids 42 (1994), pp. 1345–1374.
[13] K. Tohgo, A. Otsuka, and H.W. Gao, *The behavior of ductile crack initiation from a notch under mixed-mode loading*. Proc. Far East Fract. Gr. Work 37 (1988), pp. 101–108.
[14] Y.A. Roy, R. Narasimhan, and P.R. Arora, *An experimental investigation of constraint effects on mixed mode fracture initiation in a ductile aluminium alloy*. Acta Mater. 47 (1999), pp. 1587–1596.
[15] R. Sharma, S.V. Kamat, M. Srinivas, A.K. Singh, and P.R. Rao, *Mixed mode I/III fracture toughness in extruded magnesium alloys*. Mater. Sci. Eng. A 528 (2011), pp. 5875–5882.
[16] K.V. Vaishakh, R. Narasimhan, K.U. Yazar, and S. Suwas, *Mixed-mode (I and II) fracture behavior of a basal-textured magnesium alloy*. Acta Mater. 193 (2020), pp. 99–114.
[17] K.V. Vaishakh, and R. Narasimhan, *Numerical simulations of mixed-mode (I and II) notch tip fields in basal-textured magnesium alloys*. J. Mech. Phys. Solids 159 (2022), pp. 104717.
[18] B. Selvarajou, S.P. Joshi, and A.A. Benzerga, *Three dimensional simulations of texture and triaxiality effects on the plasticity of magnesium alloys*. Acta Mater. 127 (2017), pp. 54–72.
[19] K.V. Vaishakh, and R. Narasimhan, *On the evaluation of energy release rate and mode mixity for ductile asymmetric four point bend specimens*. Int. J. Fract. 217 (2019), pp. 65–82.

[20] ASTM E1820-08a, *Standard test method for measurement of fracture toughness*. ASTM Int. (2009), pp. 1–8.
[21] A. Sreedhar S, S. Ravindran, G. Shankar, S. Suwas, and R. Narasimhan, *Fracture mechanism and toughness of a rolled magnesium alloy under dynamic loading*. Acta Mater. 202 (2021), pp. 350–365.
[22] C. Gandhi, and M.F. Ashby, *Fracture-mechanism maps for materials which cleave: F.C.C., B.C.C. and H.C.P. metals and ceramics*. Acta Metall. 27 (1979), pp. 1565–1602.
[23] ASTM E562-19, *Standard test method for determining volume fraction by systematic manual point count*. ASTM Int. (2019), pp. 1–7.
[24] J.W. Hutchinson, *Plastic stress and strain fields at a crack tip*. J. Mech. Phys. Solids 16 (1968), pp. 337–347.
[25] S.A. Sreedhar, D. Baruah, G. Shankar, S. Suwas, and R. Narasimhan, *Temperature dependence of mode I fracture behavior of a textured magnesium alloy*. Int. J. Fract. 238 (2022), pp. 89–114.
[26] N.S. Prasad, R. Narasimhan, and S. Suwas, *Numerical simulations of cylindrical void growth in Mg single crystals*. Int. J. Fract. 200 (2016), pp. 159–183.
[27] N.S. Prasad, R. Narasimhan, and S. Suwas, *Effects of lattice orientation and crack tip constraint on ductile fracture initiation in Mg single crystals*. Int. J. Plast. 97 (2017), pp. 222–245.
[28] P.P. Indurkar, S.P. Joshi, and A.A. Benzerga, *On the micromechanics of void mediated failure in HCP crystals*. J. Mech. Phys. Solids 165 (2022), pp. 104923.